

JAN 11 '94 09:39 MSG CNTR 586-2866

P.3

MODELING OF H/O/C COMBUSTION WITH A ROBUST NAVIER-STOKES COMBUSTION CODE*

Pak-Yan Liang**, Ron L. Ungewitter**, and Merlin D. Schuman***
Rockadyne Division, Rockwell International

ABSTRACT

In an effort to create a second-generation combustion code with turnaround times fast enough to enable inclusion of CFD in the combustor design process, an efficient chemistry model for H/O/C combustion has been developed and incorporated into the pressure-based Navier-Stokes solver of the GALACSY code. The model reduces the H/O/C equilibrium reactions into a single cubic equation for the oxygen balance, and also contains a finite-rate reaction for the hydrocarbon oxidation. Comparisons with data show good predictions of all species profiles. Some unevenness exists at very low O₂ concentration levels and the cubic equation can probably be refined to overcome it.

*Work Partially Supported by NASA MSFC Contract NAS 8-40000

**Members Technical Staff, CFD Technology Center, Members AIAA

***Retired Member Technical Staff, Advanced Combustion Devices

DRAFT

INTRODUCTION

The maturation of relatively robust, general-purpose Navier-Stokes solver technology in the past decade has led to the promise that routine application of computation Fluid Dynamics (CFD) to design and analyses of combustor flow systems can now be a reality. Before that happens, however, a few remaining hurdles need to be surmounted, including:

- The generation and validation of a large selection of chemistry models covering a wide range of different levels of sophistication.
- Enhance the confidence levels in models of combustion-related turbulent transport.
- Significant advancements in the effectiveness and versatility (problem-independence) of stiffness-mitigation techniques, especially dealing with source-term stiffness in spray combustion flows.
- Broad-based anchoring of spray atomization data for different injector types.

The strategy for development of the second-generation GALACSY (General Algorithm for Analyses of Combustion Systems) family of spray combustion codes at Rocketdyne is based on the above observations. Other than substantially extending the successful pressured-based algorithm of the REACT¹ code methodology to handle transonic, multispecies and multiphase phenomena, a package of comprehensive research initiatives aimed at each of the four hurdles mentioned above is being undertaken. This report documents some of the progress being made in the particular area of chemistry model development for the combustion of methane, which can be easily extended to model the combustion of other simple hydrocarbons.

SYNOPSIS OF NUMERICAL SCHEME

Details of the numerical model are discussed in Ref. 2. For completeness, the major governing equations are listed below:

Mass:

$$\frac{\partial \bar{\rho}}{\partial t} + \nabla \cdot (\bar{\rho} \mathbf{u}) = \dot{\bar{\rho}}_d \quad (1)$$

Momentum:

$$\frac{\partial \bar{\rho} \mathbf{u}}{\partial t} + \nabla \cdot (\bar{\rho} \mathbf{u} \mathbf{u}) = -\nabla p - \nabla \left(\frac{2}{3} \bar{\rho} \bar{k} \right) + \nabla \cdot \underline{\underline{\sigma}} + \mathbf{S} + \bar{\rho} \mathbf{G} \quad (2)$$

where \mathbf{S} is the droplet coupling term, \mathbf{G} is the body force, and the viscous stress tensor is given by

$$\underline{\underline{\sigma}} = \mu [\nabla \mathbf{u} + (\nabla \mathbf{u})^T] + \lambda (\nabla \cdot \mathbf{u}) \mathbf{I} \quad (3)$$

and \bar{k} is the turbulent kinetic energy.

Internal energy:

$$\frac{\partial \bar{\rho} \bar{I}}{\partial t} + \nabla \cdot (\bar{\rho} \bar{I} \mathbf{u}) = -\bar{p} \nabla \cdot \mathbf{u} - \nabla \mathbf{J} + \bar{\rho} \epsilon + \dot{\bar{Q}}_{\text{chemistry}}^c + \dot{\bar{Q}}_{\text{spray}}^s \quad (4)$$

where the heat flux vector includes both conduction and species diffusion terms:

$$\mathbf{J} = K \nabla T - \rho_g D \sum_m h_m \nabla (\rho_m / \rho_g) \quad (5)$$

Species M:

$$\begin{aligned} \frac{\partial \bar{\rho}_m}{\partial t} + \nabla \cdot (\bar{\rho}_m \mathbf{u} \mathcal{F}) = \\ \mathcal{F} \nabla \cdot [\rho_g D \nabla \left(\frac{\bar{\rho}_m}{\rho_g} \right)] + \dot{\bar{\rho}}_{\text{chemistry}}^c + \dot{\bar{\rho}}_s \delta_{m,s} \text{evaporation} \end{aligned} \quad (6)$$

Turbulent Kinetic Energy:

$$\begin{aligned} \frac{\partial \bar{\rho} \bar{k}}{\partial t} + \nabla \cdot (\bar{\rho} \mathbf{u} \bar{k}) = \\ -\frac{2}{3} \bar{\rho} \bar{k} \nabla \mathbf{u} + \underline{\underline{\sigma}} : \nabla \mathbf{u} + \nabla \cdot \left[\frac{\mu}{c_k} \nabla \bar{k} \right] - \bar{\rho} \epsilon + \dot{\bar{W}}_s \text{droplet} \\ \text{turbulence suppression} \end{aligned} \quad (7)$$

Turbulent Dissipation:

$$\begin{aligned} \frac{\partial \bar{\rho} \bar{\epsilon}}{\partial t} + \nabla \cdot (\bar{\rho} \mathbf{u} \bar{\epsilon}) = -(\frac{2}{3} c_1 - c_3) \bar{\rho} \bar{\epsilon} \nabla \mathbf{u} + \nabla \cdot \left[\frac{\mu}{c_\epsilon} \nabla \bar{\epsilon} \right] + \\ \frac{\bar{\epsilon}}{k} [c_1 \underline{\underline{\sigma}} : \nabla \mathbf{u} - c_2 \bar{\rho} \bar{\epsilon} + c_s \dot{\bar{W}}_s] \end{aligned} \quad (8)$$

Volume Fraction:

$$\frac{\partial \mathcal{F}}{\partial t} + \nabla \cdot \mathbf{u} \mathcal{F} = \dot{\mathcal{F}}_s \quad (9)$$

where

$$\mathcal{F} = V_g / (V_g + V_l) \quad (10)$$

The volume fraction equation (9) arises because GALACSY is designed to handle an additional immiscible liquid phase (which is incompressible and chemically inert) using the Volume-of-Fluid (VOF) cell-participating technique³. Equations (7) through (9) were not activated for purposes of this study. Note that the conservation equations are also written for the per unit total mass (cell average) variables, defined as

$$\bar{\rho} = \mathcal{F}\rho_g + (1-\mathcal{F})\rho_l \quad (11)$$

$$\bar{I} = \frac{\rho_g \mathcal{F} I_g + \rho_l (1-\mathcal{F}) I_l}{\bar{\rho}} \quad (12)$$

which defaults back to the simple gaseous variables when no liquid phase is present. This system of equations is then closed with the multispecies perfect gas equation and simple summation rules for the gas mixture. Real gas property data (enthalpy, heat of formation, etc.) in the form of JANNAF tables are automatically included into the program from library files.

GALACSY uses a sequential solver based on extensions of the SIMPLE⁴ approach, as highlighted in Figure 1. In the steady-state version, all source terms (evaluated with the aid of various physical submodels) must be supplied to the main subroutines in terms of changes per unit time. As indicated in the flow chart, up to four major subroutines can be involved in the current chemistry/species diffusion submodel. CHEMKN contains a general-purpose package⁵ for solving Arrhenius-type kinetic rate equations, and is called by subroutine CALCSP. The latter is invoked to solve the species conservation equation, eq. (7), for species designated as "kinetic" species by the user or for all species if no chemistry is involved. It also evaluates the heat flux terms due to species diffusion for those species. On the other hand, for those species that are designated as "equilibrium" species controlled by fast reactions, no such thing as an effective reaction rate exists in steady-state, and the species composition at any point is dictated by the balance of convective and diffusive fluxes of the available atomic species. Hence, CALCEQ is invoked to solve for the conservation of the total atomic species rather than the equilibrium compounds, and then CHEMEQ executes the chemistry model to solve for the molar composition based on the atomic totals available. However, as in the case of CALSCP, CALCEQ does evaluate the heat flux terms due to species diffusion for each and every equilibrium compound species.

DRAFT

THE H/O/C CHEMISTRY MODEL

Previous experience (e.g., Ref. 5) has shown that the chemistry portion of a typical combustion simulation can take upwards of 30% of the overall computational time even if only a relatively simple set of equilibrium reactions were involved, and more if a detailed set of kinetic reactions were used. The need to invert a coefficient matrix for equilibrium reactions at every iteration or time step makes a general purpose equilibrium chemistry package such as CHEMEQ in Ref. 6 inherently time-consuming. It is observed that for the majority of combustion applications, the core of the chemistry model consists of the hydrogen-oxygen reactions which are almost always fast enough compared to the fluid dynamic time scales to be considered equilibrium reactions. These reactions can then be augmented with finite-rate hydrocarbon oxidation or nitrogen kinetic reactions as needed. Furthermore, it is observed that the internal flame structure is typically dominated by the availability of oxygen atoms at a particular point, and thus a timely general equilibrium chemistry package is not necessary. The following model thus takes advantage of these observations to reduce the hydrogen-oxygen reactions into a single cubic equation for oxygen concentration, which can be solved very efficiently. All other O/H species can then be algebraically evaluated, making the overall chemistry calculations extremely fast.

Consider the following set of equilibrium reactions:



where the K's are the equilibrium constants and the chemical symbols in parentheses represents molar concentrations. Note that the right hand portions of eqs. (13) through (18) apply only at equilibrium. Now the hydrogen balance at the beginning of the equilibrium calculations (designated by subscript o), excluding the hydrogen contained in the hydrocarbon fuel is given by

$$(\hat{H})_o = 2 (H_2) + 2 (H_2O) + (OH) + (U) + (HO_2) + 2 (H_2O_2) \quad (19)$$

$$= (\rho_H)_{total} - m (\rho_{HC}) \quad (19a)$$

where m is the number of hydrogen atoms in the hydrocarbon fuel, and HC is the generic hydrocarbon. (For methane, m = 4.) This number does not change as the composition evolves toward equilibrium.

DRAFT

Let

$$\alpha_H \equiv \frac{1}{2} \left[(\hat{H})_O - (OH) - (HO_2) - 2 (H_2O_2) \right] \quad (20)$$

Substituting equation (20) into equation (19) yields

$$(H_2) + (H_2O) = \alpha_H \quad (21)$$

Substituting equation (13) into equation (21) yields

$$(H_2) + (KH_2O) (\sqrt{O_2}) (H_2) = \alpha_H \quad (22)$$

or

$$(H_2) = \frac{\alpha_H}{1 + (KH_2O) (\sqrt{O_2})} \quad (23)$$

Similarly, the oxygen balance is given by

$$(\hat{O})_O = 2 (O_2) + (H_2O) + (OH) + 2 (HO_2) + 2 (H_2O_2) + (O) + (CO) + 2 (CO_2) \quad (24)$$

$$= (\rho_O)_{\text{total}} - n (\rho_{HC}) \quad (24a)$$

where n is the number of oxygen atoms in the hydrocarbon fuel (for methane, n = 0).

Again, let

$$\alpha_O \equiv (\hat{O})_O - (OH) - 2 (HO_2) - 2 (H_2O_2) \quad (25)$$

Substituting equation (25) into equation (24) yields

$$2(O_2) + (H_2O) + (CO) + 2(CO_2) = \alpha_O \quad (26)$$

where (CO and (CO₂) will have nonzero values if a hydrocarbon fuel is involved. In that case, the CO/CO₂ shift equilibrium must be introduced, which is

DRAFT

$$\text{CO} + \text{H}_2\text{O} \rightleftharpoons \text{CO}_2 + \text{H}_2 ; \quad (\text{CO}_2) = (K_{\text{shift}}) \frac{(\text{H}_2\text{O}) (\text{CO})}{(\text{H}_2)}$$

The carbon balance, again excluding the unburned fuel, is

$$(\hat{\text{C}})_o = (\text{CO}) + (\text{CO}_2) \quad (28)$$

$$= (\rho_C)_{\text{total}} - q (\rho_{\text{HC}}) \quad (28a)$$

where q is the number of carbon atoms in the hydrocarbon. (For methane, $q = 1$.)

Combining eqs. (27) and (28) and rearranging leads to

$$(\text{CO}) = \frac{(\hat{\text{C}})_o (\text{H}_2)}{(\text{H}_2) + (K_{\text{shift}}) (\text{H}_2\text{O})} \quad (29)$$

and

$$(\text{CO}_2) = \frac{\hat{\text{C}}_o (K_{\text{shift}}) (\text{H}_2\text{O})}{(\text{H}_2) + (K_{\text{shift}}) (\text{H}_2\text{O})} \quad (30)$$

Note that if $(\text{H}_2) = 0$ and $(\text{H}_2\text{O}) = 0$, then CO_2 should be zero and (CO) set equal to $(\hat{\text{C}})_o$.

Substituting eqs (29), (30) and (13) back into (26) yields

$$2 (\text{O}_2) + (K_{\text{H}_2\text{O}}) (\text{H}_2) (\sqrt{\text{O}_2}) + \left[\frac{(\text{H}_2) + 2 (K_{\text{shift}}) (\text{H}_2)}{(\text{H}_2) + (K_{\text{shift}}) (\text{H}_2\text{O})} \right] (\hat{\text{C}})_o = \alpha_o \quad (31)$$

Now define

$$\beta = \frac{(\text{H}_2) + 2 (K_{\text{shift}}) (\text{H}_2\text{O})}{(\text{H}_2) + (K_{\text{shift}}) (\text{H}_2\text{O})} ; \quad 1 \leq \beta \leq 2 \quad (32)$$

where β should be set to 1 if $(\text{H}_2) = 0$ and $(\text{H}_2\text{O}) = 0$,

DRAFT

and substituting it into eq. (31) gives

$$2 (O_2) + (KH_2O) (\sqrt{O_2}) (H_2) + (\beta) (\hat{C})_O = \alpha_O \quad (33)$$

Finally, combined the hydrogen balance equation (23) with (33) yields, after some manipulation, the cubic equation for oxygen

$$\begin{aligned} & (\sqrt{O_2})^3 [(2) (KH_2O)] + (\sqrt{O_2})^2 [(2)] + (\sqrt{O_2}) (KH_2O) [(\beta) (\hat{C})_O - \alpha_O + \alpha_H] \\ & + [(\beta) (\hat{C})_O - \alpha_O] = 0 \end{aligned} \quad (34)$$

Thus the H/O/C equilibrium calculations start with evaluation of all the K values at the cell temperature, which are assumed to be of the form

$$K = \exp\{A \ln T_A + B/T_A + C + DT_A + ET_A^2\} \quad (35)$$

in the data library, and where $T_A = T/1000$. The variables α_H , α_O and β are then calculated and the cubic root for the oxygen equation sought. If more than one real positive root which also meets the criterion $(\sqrt{O_2})^2 \leq (\hat{O})_O$ exists, then the smallest root is picked if the cell is in a hydrogen-rich zones, i.e., if $(\hat{H})_O < (\hat{O})_O$. Otherwise the largest root is picked. Once the oxygen concentration is known, the hydrogen concentration follows from eq. (23) and all other equilibrium species can be determined from the equilibrium constants.

Up to this point the finite rate oxidation step of the hydrocarbon fuel has been let out. That rate, in terms of moles of CH₄ depleted per unit time per unit volume, is expressed as a one-way, single-step reaction

$$(\dot{\rho})_{HC}^c = -k_{HC} (\rho_{HC})^a (\rho_{O_2})^b \quad (36)$$

where

$$k_{HC} = A_{HC} T^\zeta e^{-E_{HC}/RT} \quad (37)$$

and a, b specify the effective order of the reaction. (For the methane test case below, the values used are

DRAFT

$A_{HC} = 1 \times 10^{13}$, $\zeta = 0$, $E_{HC} = 1.578 \times 10^4$, $a = 0.25$ and $b = 1.5$ in cgs units).

The overall procedure for solving the species composition can now be summarized as follows:

- Step A** Including eq. (36) as a source term, solve the hydrocarbon species conservation equation in CALSCP.
- Step B** Solve the atomic species conservation equations for $(\rho_C)_{total}$, $(\rho_H)_{total}$ and $(\rho_O)_{total}$ in CALCEQ.
- Step C** Evaluate the $(\hat{C})_O$, $(\hat{H})_O$, $(\hat{O})_O$ subtotals at end of CALCEQ
- Step D** Go on with the rest of H/O/C equilibrium calculations in CHEMEQ.

SAMPLE TEST CASE

To validate the current H/O/C chemistry model as well as the overall gaseous combustion capabilities of the GALACSY code, the diffusion flame experiment by Mitchell⁷ et al has been chosen as a benchmark test case. In this confined, coflowing methane-air experiment the flame was probed extensively to obtain detailed species concentration profiles. Furthermore, the laminar nature of the flow removes one of the biggest sources of uncertainty in all CFD simulations and especially in combustion cases – that due to turbulence modeling. Figure 2 contains a schematic of the laboratory burner taken from Ref. 7 as well as the 41×101 (2.54 cm x 30 cm) axisymmetric grid used in the present computations. Table 1 summarizes the pertinent flow parameters. In the numerical model, a total of 12 species (O, C, H, N₂, CH₄, O₂, H₂, CO₂, H₂O, CO, HO₂, H₂O₂) are tracked including the inert N₂ species, even though the atomic C species is not involved with any reactions. For boundary conditions, all quantities are specified at the inflow plane, a constant pressure of 1.01296×10^6 dynes/cm² is specified at the outflow plane, symmetry axis is used at the centerline, and adiabatic no-slip conditions are used at the outer cylinder wall. Gravity is included because the problem is largely one of natural convection. The computational domain is initialized to be prefilled with air (76.1% N₂ by weight).

Laminar viscosity throughout is evaluated using Sutherland's formula

$$\mu_{lam} = 1.457 \times 10^{-5} T^{3/2}/(T+110.) \text{ poise} \quad (38)$$

where the empirical coefficients are those for air. As it turned out, final species and temperature profile predictions are quite sensitive to the respective diffusion coefficients, and hence to the effective Schmidt and Prandtl numbers. Using constants for all points of different compositions was clearly inadequate. As a first order refinement, the following formula is used:

DRAFT

$$\frac{1}{P_r} = \frac{1}{S_c} = \frac{C_p + 2.25R}{C_p} \quad (39)$$

where R is the local gas constant and C_p is the local specific heat at constant pressure.

In the course of the computations, it was also discovered that recirculating backflow can occur across the exit plane towards the outer wall. This reverse flow can make impossible convergence

Table 1
Summary of Flow Parameters for Methane Burner

	Inner Tube	Outer Tube
Radius	$r_o = 0.635 \text{ cm}$	$R_o = 2.54 \text{ cm}$
Velocity	$U_{\text{fuel}} = 4.50 \text{ cm/s}$	$U_{\text{air}} = 9.88 \text{ cm/s}$
Vol Flow Rate	$\dot{V}_{\text{fuel}} = 5.7 \text{ cc/s}$	$\dot{V}_{\text{air}} = 187.7 \text{ cc/s}$
Inflow Pressure	$1.013 \times 10^6 \text{ dynes/cm}^2$	$1.013 \times 10^6 \text{ dynes/cm}^2$
Inflow Temperature	298 deg. K	298 deg. K

to the steady-state solution. Thus, it was found necessary to eliminate this backflow by gradually increasing the viscosity value toward the exit. This was done for cells of $I > 60$ ($X > 12 \text{ cm}$). Since all flow features of interest are located upstream of $X = 7 \text{ cm}$, this treatment should not significantly impact the accuracy of the results.

Figures 3 through 7 highlight the computed results as well as their comparison with data. As can be seen in Fig. 3b, the rapid heat-up of the central jet results in a large acceleration of the center stream and a compensating reverse flow of air near the wall, although this recirculation zone is terminated by the artificial increase of viscosity towards the exit. The species contours all show a well-defined conical flame shape with a slight radial expansion at the base of the flame. CH_4 consumption is virtually complete by $X = 6 \text{ cm}$.

Quantitative comparison of radial profiles at three axial locations are presented in Figs. 5, 6, and 7. The following observations can be made:

1. The major species of O_2 , H_2O and CO_2 are generally quite well predicted, especially on the air side of the flame. A dip in the predicted CO_2 profile in the mid-radius range inside of the flame envelope corresponds to an overprediction of the minor species H_2 and CO in the same region. This may be because of inaccuracies in the H_2 evaluation based on eq. (23) when oxygen concentration is low, ($K_{\text{H}_2\text{O}}$ being a vary large number), which in turn leads to inaccuracies in CO and CO_2 by way of the shift equilibrium eqs. (27) and (28). H_2O prediction is not much affected by this problem

DRAFT

because, as can be seen in eq. (13), (H_2O) will be well predicted as long as $(\text{H}_2) \sqrt{\text{O}_2} \approx \alpha_{\text{H}}/(\text{KH}_2\text{O})$ is properly evaluated.

2. CH_4 concentration is overpredicted especially toward the centerline, though agreement is still better than obtained with the model by Mitchell et al in Ref. 7. (See discussion on Fig. 8 below). This, together with the high values of (CO) and (H_2) , corresponds with a low value of (N_2) in the flame zone. A possible explanation may be insufficient diffusion rates for nitrogen, or for oxygen, or both. A larger methane diffusion rate can presumably reduce (CH_4) also, but the temperature plots show that the "flame front," as indicated by the temperature maximum, is already to the outside of the measured locations.
3. The peak temperature as well as the centerline temperatures are generally overpredicted by about 10%, which causes overpredictions on the velocity profiles as well. The source of this discrepancy can be two fold. First, for the partial species internal energy in the energy conservation equation, the sensible energy which includes the heat of formation is currently used instead of the absolute energy (referenced to absolute zero) which does not include the heat of formation. The advantage is that no energy source term would arise due to chemical reactions; the change in temperature would be backed out from the change in composition alone. The potential disadvantage is that because the different species have vastly different heats of formation, minute inaccuracies in some species can lead to large inaccuracies in temperature. Second, since energy and not temperature is the conservation variable in eq. (4), the heat conduction term would have to be expressed in terms of energy as well in keeping with the practice in the rest of the program to difference the diffusion term implicitly. This leads to additional correction terms involving gradients of the specific heats which again can be very steep and inaccurate to compute in multispecies flows. Both of these sources of error will be systematically investigated in the future.
4. The temperature, CO_2 and H_2O all show a "kink" in their profiles near the peaks. The cause of this problem is unclear, though the kink is less severe than when equilibrium chemistry was also used for CH_4 in some preliminary calculations not reported here. Because its location is where oxygen concentration practically goes to zero, inaccuracy in the $(\sqrt{\text{O}_2})$ cubic root at such point may again be the culprit.
5. Examination of the O_2 and CH_4 profiles shows that there is a region where uncombusted O_2 and CH_4 coexist, which may be interpreted as the flame zone. The thickness of this region is small, however, (less than 0.2 cm), which agrees with the experimentally observed thickness of the blue reaction zone. This explains the relative success of earlier computations all using Burke and Schumann's⁸ flame-sheet concept where the reaction between fuel and air is infinitely fast and one-way. This would not be the case at elevated pressures or if fuels that oxidize more slowly were used, or if turbulence disrupts the diffusion flame front. In such cases the need for a realistic set of chemical reactions fully coupled with fluid dynamics, as attempted here, will be more pronounced.

Figure 8 repeats some of the currently computed results and data and compares them with the theoretical values computed by Mitchell⁷ et. al. Except for temperature, the current results are generally superior. CO and H_2 were not included at all in Mitchell's

DRAFT

model, and his (CH_4) values at centerline are much too high. His modified flame-sheet model allows zero mutual penetration of the CH_4 and O_2 species.

6. Finally, in Fig. 9, several contours of the effective stoichiometric oxygen coefficient are plotted. The experimentally observed luminous flame core closed on the axis at 5.8 cm above the burner plate. According to Ref. 7, this core represents the inner edge (circles) of the blue reaction zone associated with burnout of CO, whose outer edge is represented by squares. The best fit for the circles is the contour with a value of 2.2, and the squares contour 2.3. This contrast with the predicted values of 1.76 and 2.0 in Ref. 7. Since 2.0 is the theoretical value for complete stoichiometric combustion it indeed should correspond to the burnout of CO and the outer edge of the blue zone. Corroboration with Fig. 7 shows that this higher value is an immediate result of overpredicted values of CO and H_2O , both of which in turn can be traced to an overprediction of H_2 in the low (O_2) region. Thus, improvements in this regime of the oxygen cubic equation is called for.

CONCLUSIONS

The benchmark test case has confirmed that the simplified H/O/C combustion model is indeed capable of good species concentration predictions. For further refinement, three areas present themselves for investigation:

1. More sophisticated formulas for the effective Schmidt and Prandtl numbers to capture the varying diffusion rates for different species.
2. A switch of variable for the energy conservation equation, from sensible energy to absolute internal energy to increase accuracy of temperature predictions, and possibly alternative treatment of the heat conduction term.
3. Refine the root selection process for the oxygen cubic equation at low (O_2) levels to ensure a smoother (O_2) profile.

In addition, future activities will also include application of the model to turbulent combustion flows.

ACKNOWLEDGEMENT

The authors wish to thank Dr. P. McConnaughey and Mr. K. Tucker at MSFC for their continued support and direction of the GALACSY code development effort.

DRAFT

REFERENCES

1. Chan, D.C., Hadid, A.H., and Sindir, M.M., "On the Development of a Reynolds-Averaged Navier-Stokes Solver for Turbomachinery," Proc. 2nd. Int. Symp. on Transport Phenomena, Dynamics and Design of Rotating Machinery, Apr. (1988).
2. Liang, P.Y. and Chan, D.C., "Development of a Robust Pressure-Based Numerical Scheme for Spray Combustion Applications," AIAA-93-0902, (1993).
3. Hirt, C.W. and Nichols, B.D., "Volume of Fluid (VOF) Method for the Dynamics of Free Boundaries," J. Comp. Phy., vol. 39, no. 1, (1981), pp. 201-225.
4. Patankar, S.V. and Spalding, D.B., "A Calculation Procedure for Heat, Mass and Momentum Transfer in Three-Dimensional Parabolic Flows," Int. J. Heat Mass Transfer, vol. 15, (1972), p. 1787.
5. Liang, P. and Ungewitter, R., "Multi-Phase Simulations of Coaxial Injector Combustion," AIAA-92-0345, Jan. (1992).
6. Cloutman, L.D., Dukowicz, L.K., Ramshaw, J.D., and Amsden, A.A., "CONCHAS-SPRAY: A Computer Code for Reactive Flows with Fuel Spray," LA-9294-MS Los Alamos Nat. Lab., May (1982).
7. Mitchell, R.E., Sarofim, A.F., and Clomburg, L.A., "Experimental and Numerical Investigation of Confined Laminar Diffusion Flames," Combustion and Flame, Vol. 37, pp. 227-244, (1980).
8. Burke, S.P. and Schumann, T.E.W., Indust. Eng. Chem., vol. 29, (1928), p. 998.

D R A F T

LIST OF FIGURES

FIGURE

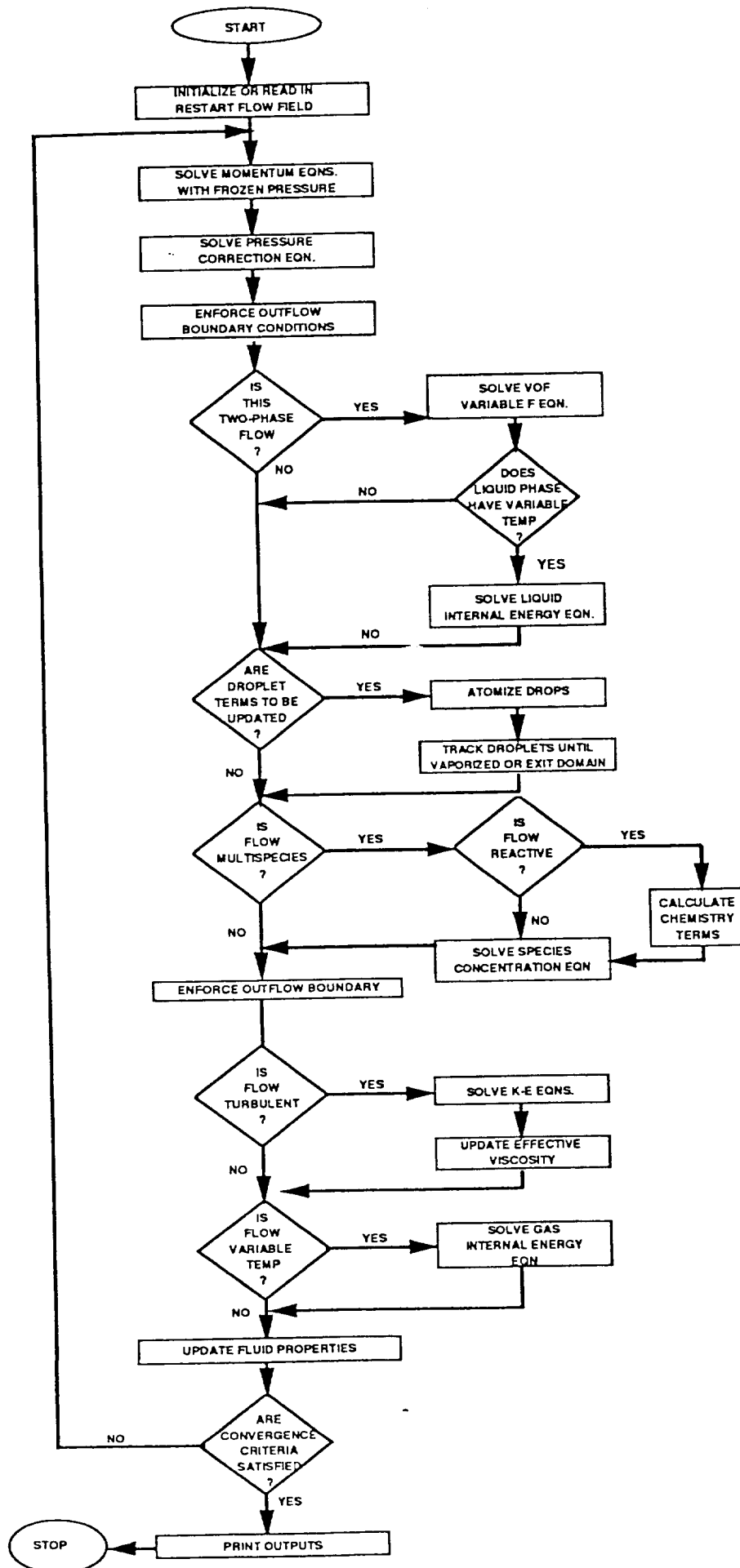
- 1 Flow Chart of GALACSY Algorithm
- 2a Schematic of Methane Burner
- 2b Computational Grid
- 3a Temperature Contours
- 3b Velocity Vector Plot
4. Species Molar Concentration Contours of CH₄, H₂O, CO and CO₂.
5. Concentration, Temperature and Velocity profiles at 1.2 cm Above the Burner Plate
6. Concentration, Temperature and Velocity profiles at 2.4 cm Above the Burner Plate
7. Concentration, Temperature and Velocity profiles at 5.0 cm Above the Burner Plate
8. Selected Reactant and Product Species Profile Comparisons at 1.2 cm Between GALACSY, Model of Mitchell et al., and Data
9. Laminar Flame Shape Comparisons

TABLES

TABLE

- 1 Summary of Flow Parameters for Methane Burner

OVERALL FLOW CHART FOR ASCOMB GALACSY



KEY SUBROUTINES

MODINP

CALCUV

CALCP

OUTBC

CALCF

CALCENL

ATOMIZ
PTRACK

EVAP
PFIND

CALCSP
CHEMKN
CALCEQ
CHEMEQ
OUTBC

CALCSC (ITE)
CALCSC (IED)

MODVIS

CALCSC (IEN)
TEMPER

MODPRO

PRINT

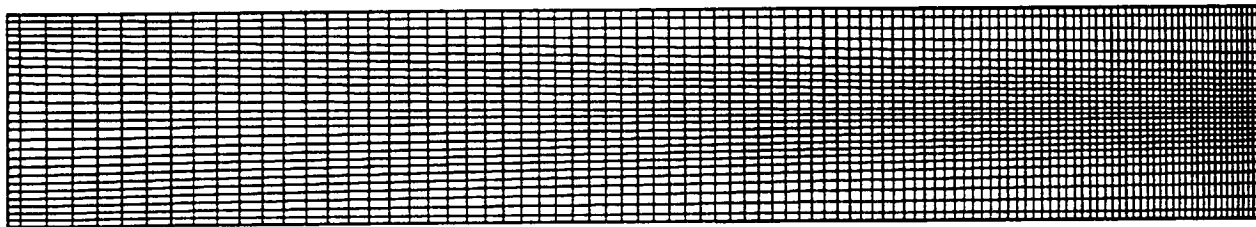
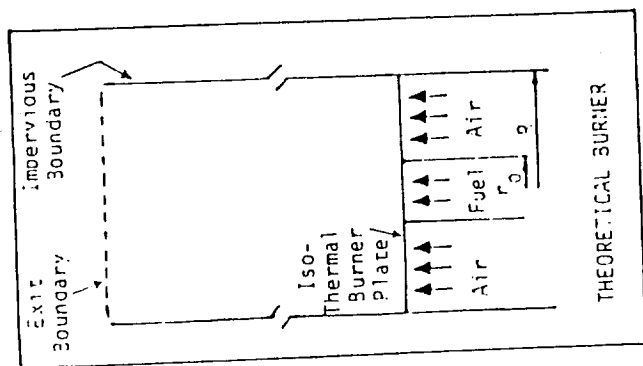
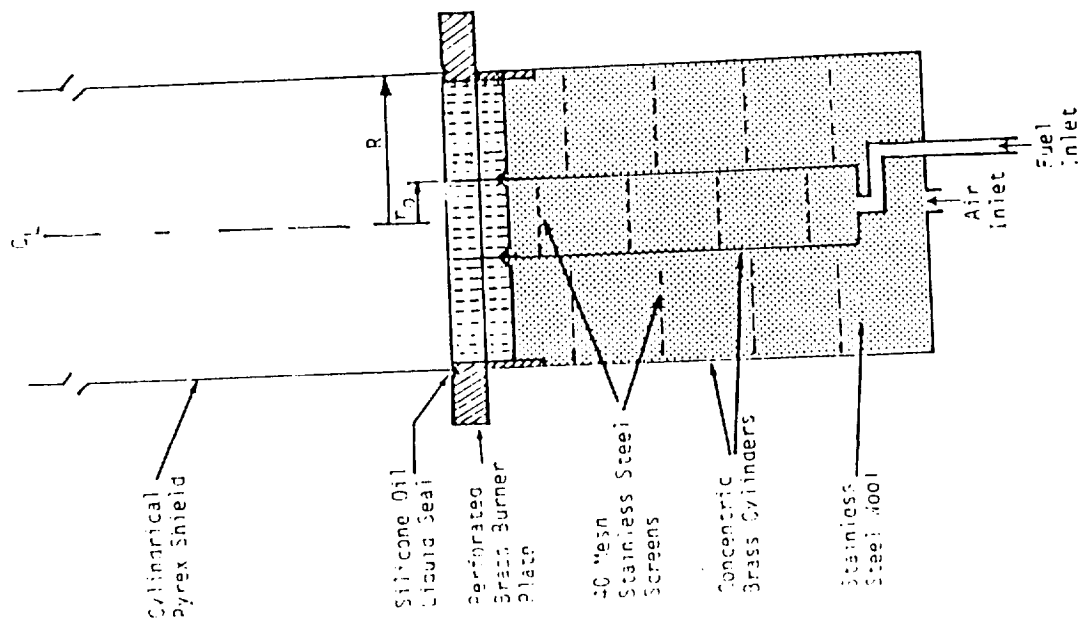
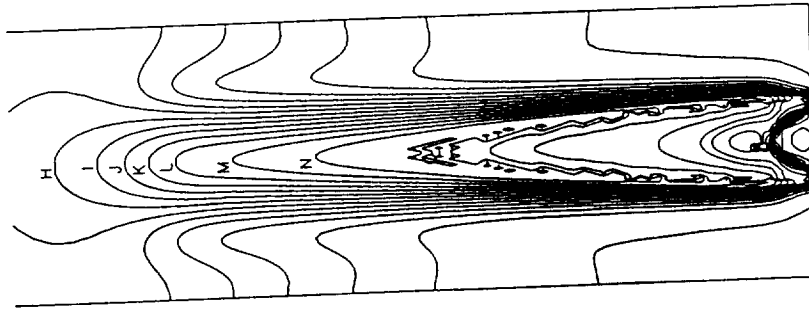


Fig. 2

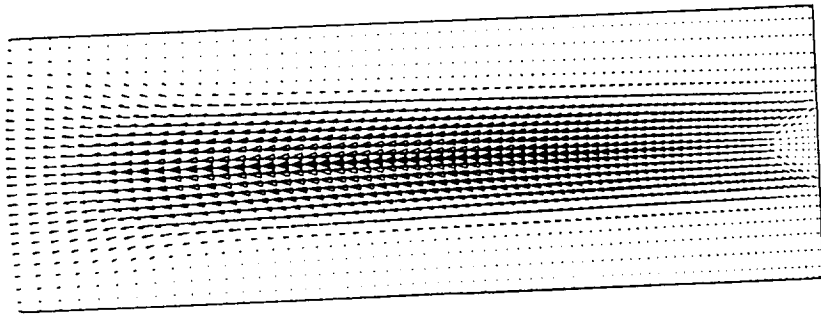
GALACSY SIMULATION Axisymmetric Laminar Methane-Air Flame



Temperature

A	300
B	450
C	600
D	750
E	900
F	1050
G	1200
H	1350
I	1500
J	1650
K	1800
L	1950
M	2100
N	2250
O	2400

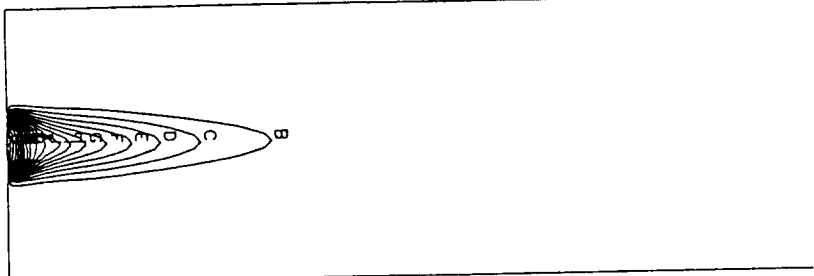
GALACSY SIMULATION Axisymmetric Laminar Methane-Air Flame



Every other radial Vector

Fig 3

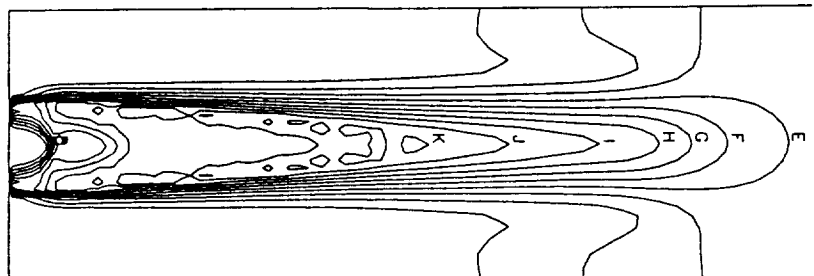
GALACSY SIMULATION Axisymmetric Laminar Methane-Air Flame



CH4 Molar Concentration

A	0.00
B	0.05
C	0.10
D	0.15
E	0.20
F	0.25
G	0.30
H	0.35
I	0.40
J	0.45
K	0.50
L	0.55
M	0.60
N	0.65
O	0.70
P	0.75
Q	0.80
R	0.85
S	0.90
T	0.95
U	1.00

GALACSY SIMULATION Axisymmetric Laminar Methane-Air Flame



H2O Molar Concentration

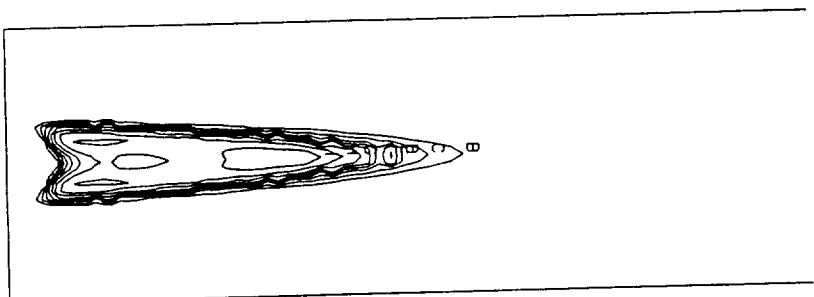
A	0.00
B	0.02
C	0.04
D	0.06
E	0.08
F	0.10
G	0.12
H	0.14
I	0.16
J	0.18
K	0.20
L	0.22

Fig. 4

a

b

GALACSY SIMULATION Axisymmetric Laminar Methane-Air Flame

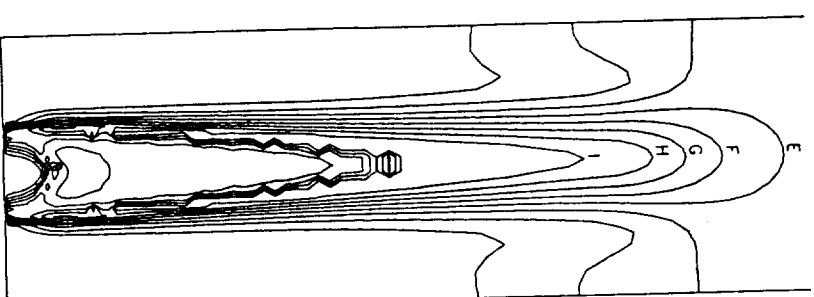


CO Molar Concentration

A	0.00
B	0.01
C	0.02
D	0.03
E	0.04
F	0.05
G	0.06
H	0.07
I	0.08
J	0.09

(c)

GALACSY SIMULATION Axisymmetric Laminar Methane-Air Flame



CO2 Molar Concentration

A	0.00
B	0.01
C	0.02
D	0.03
E	0.04
F	0.05
G	0.06
H	0.07
I	0.08
J	0.09

(d)

Fig 4 (contd)

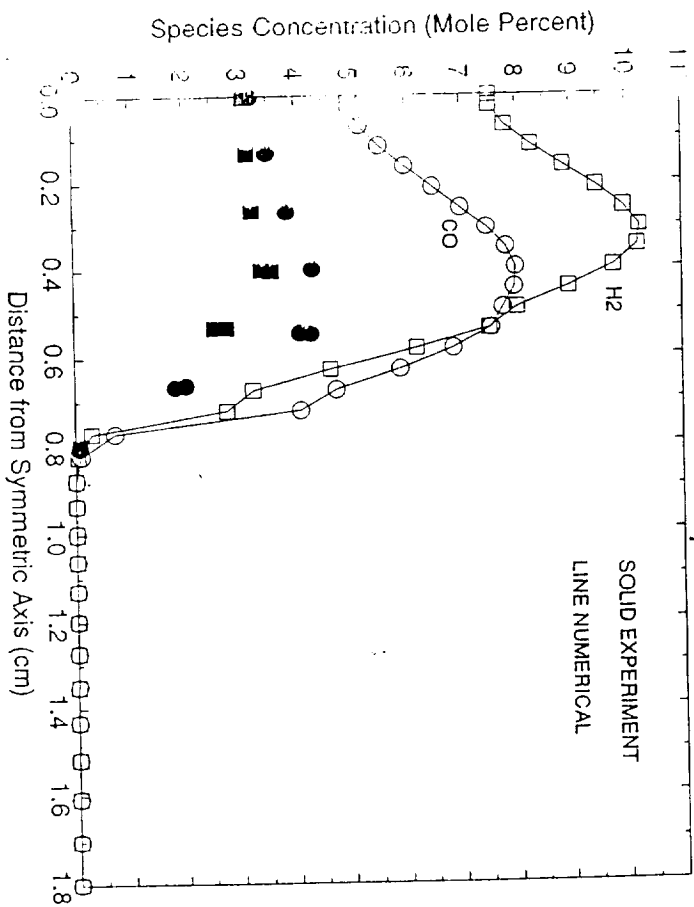
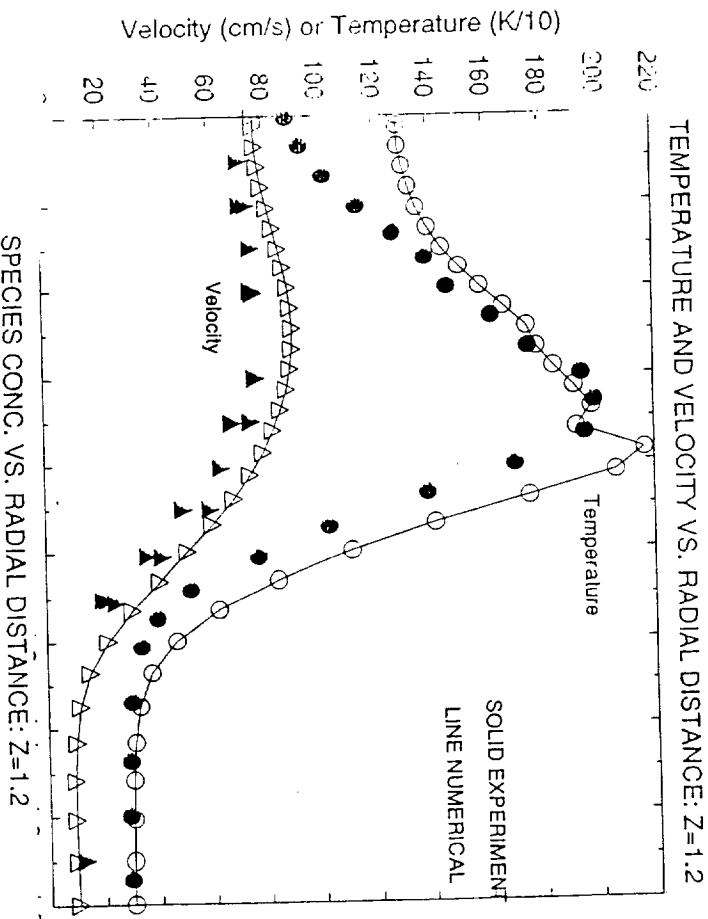
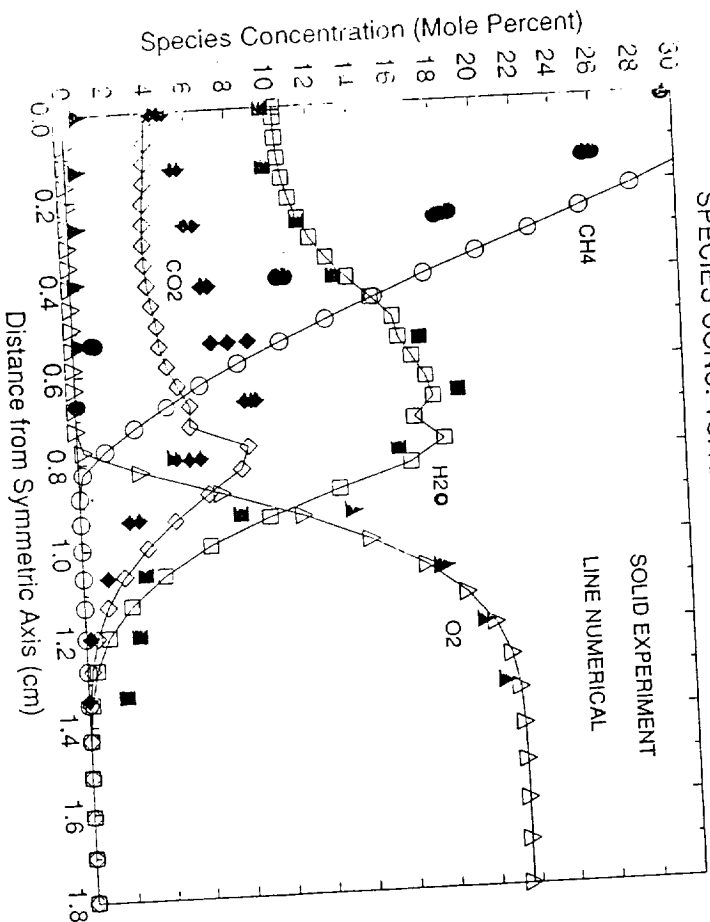
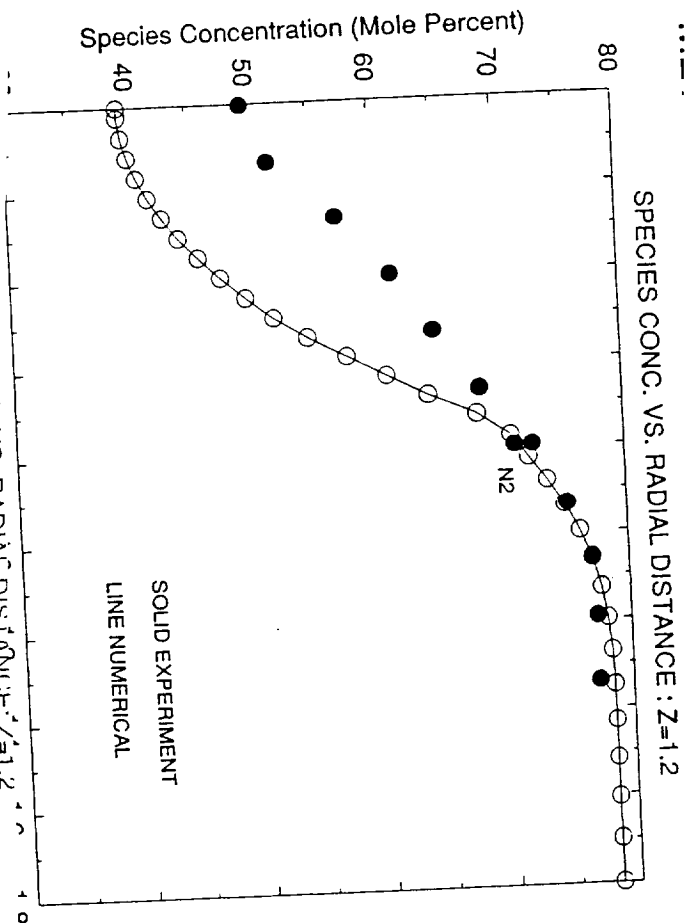


Fig. 5

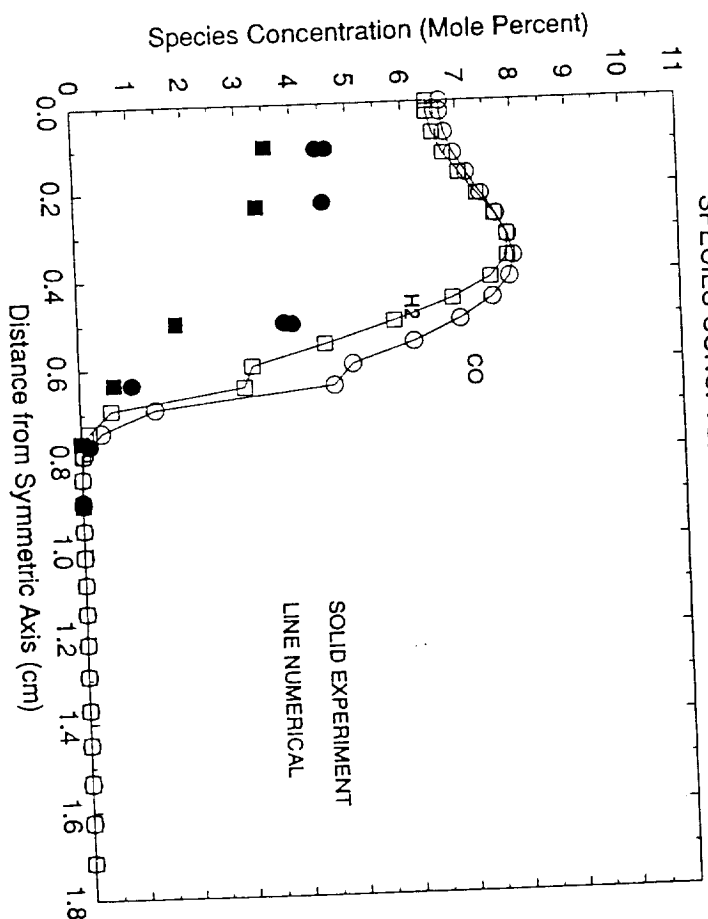
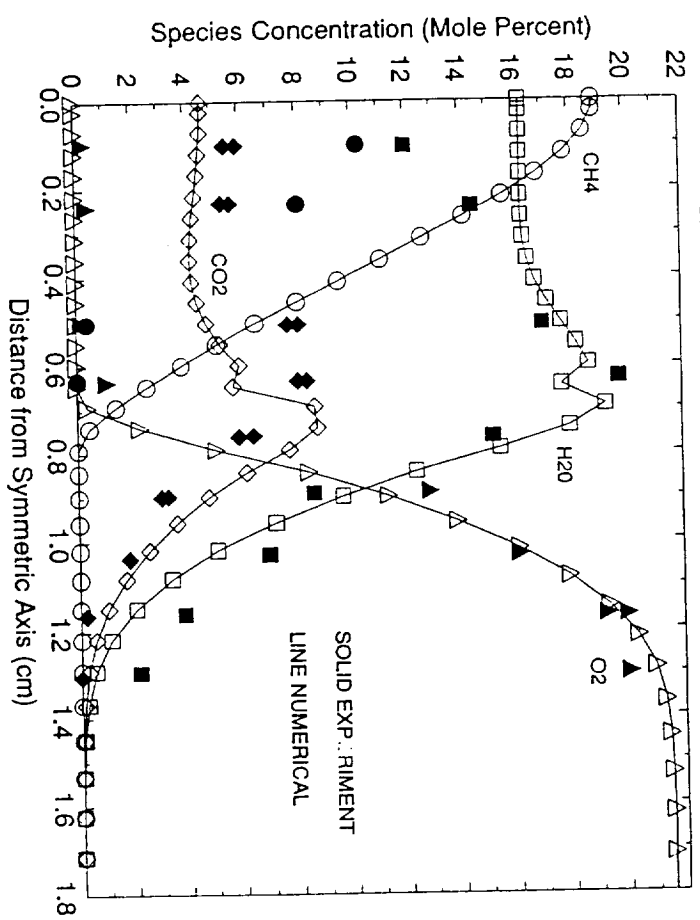
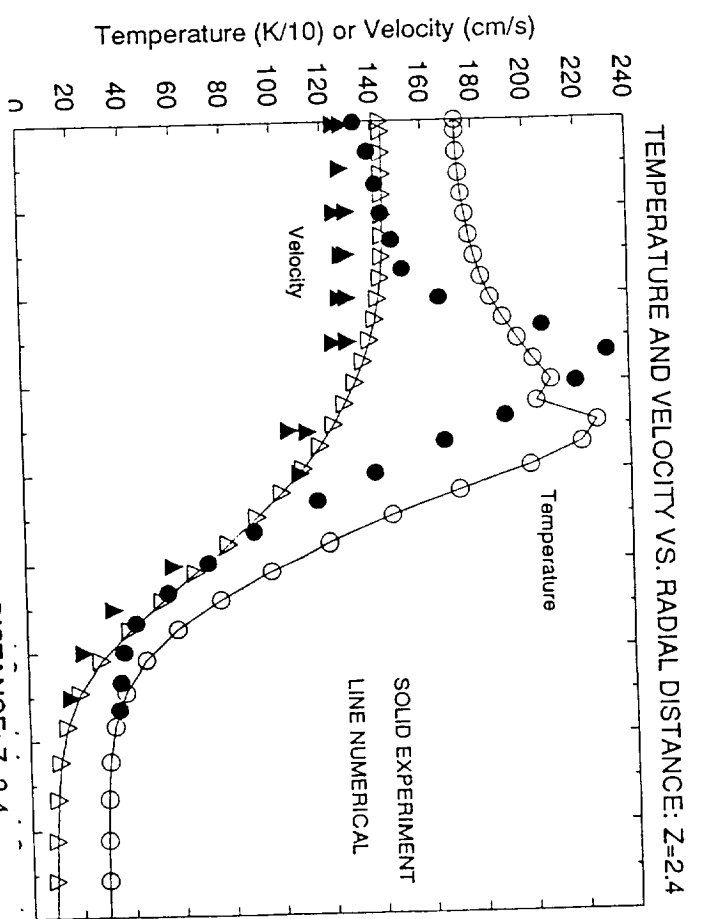
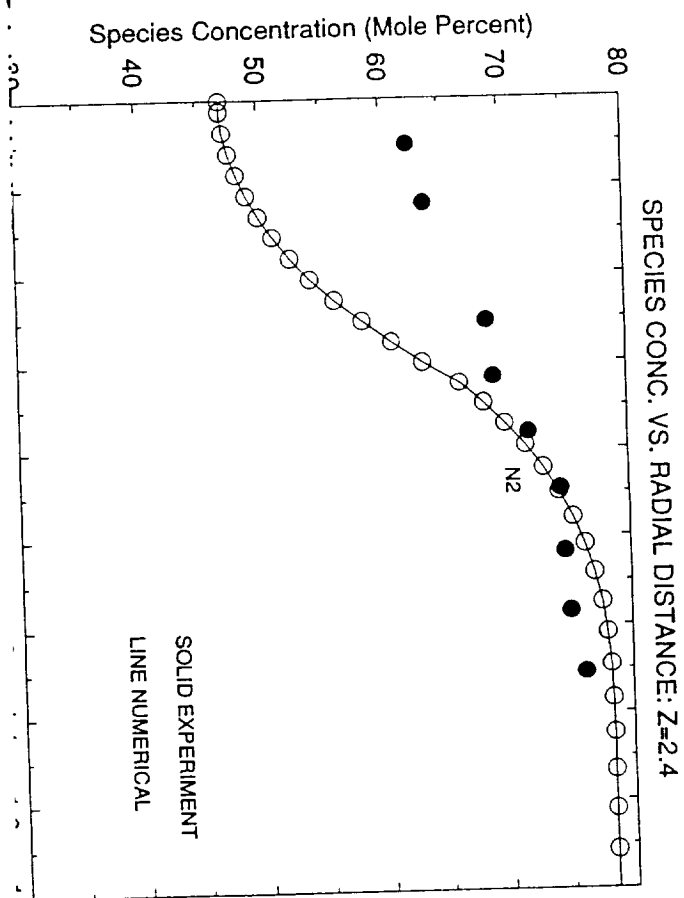
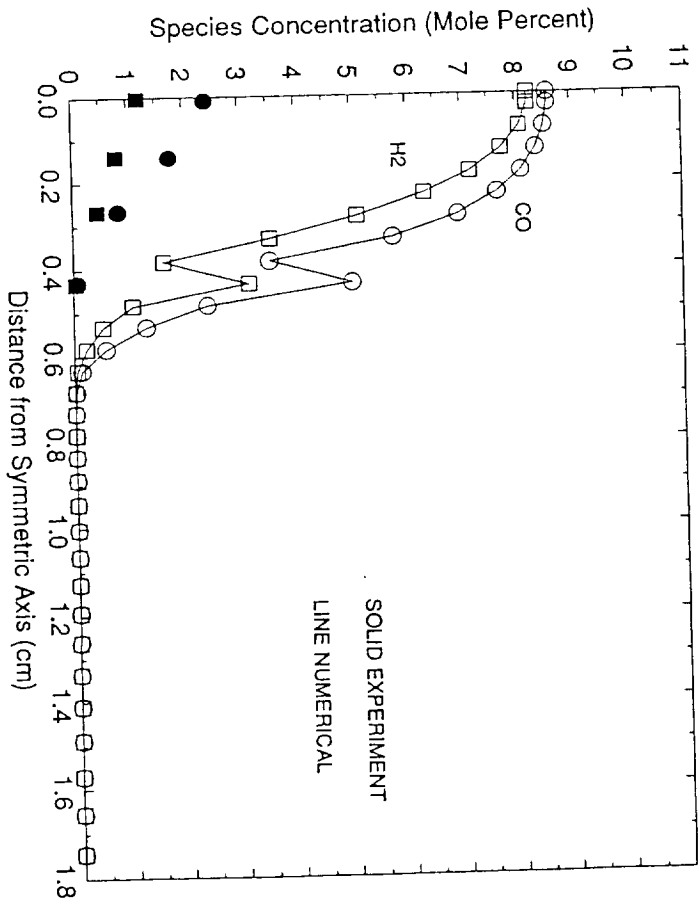
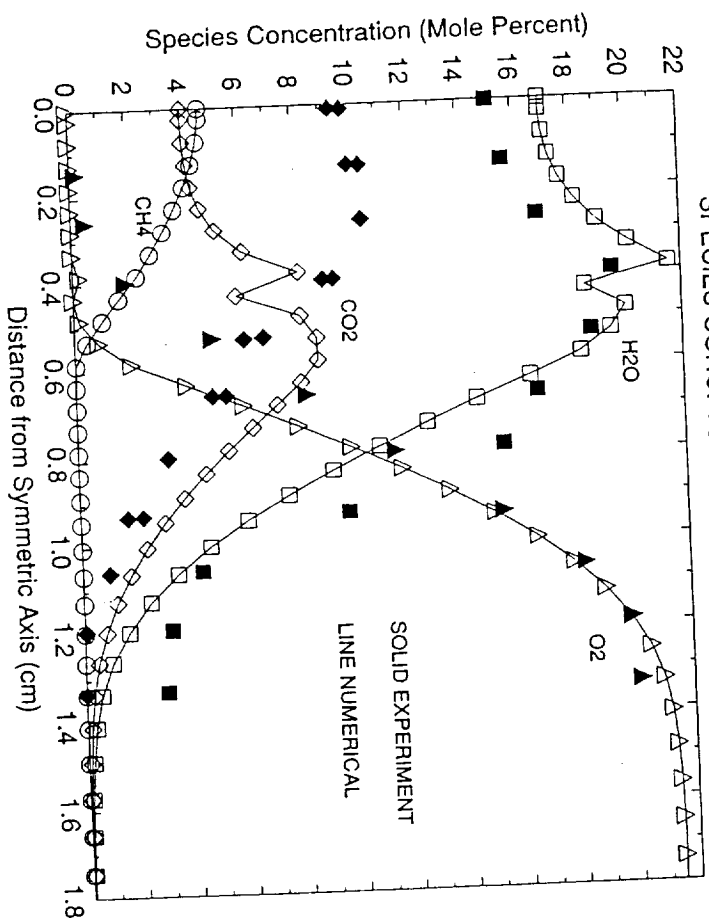
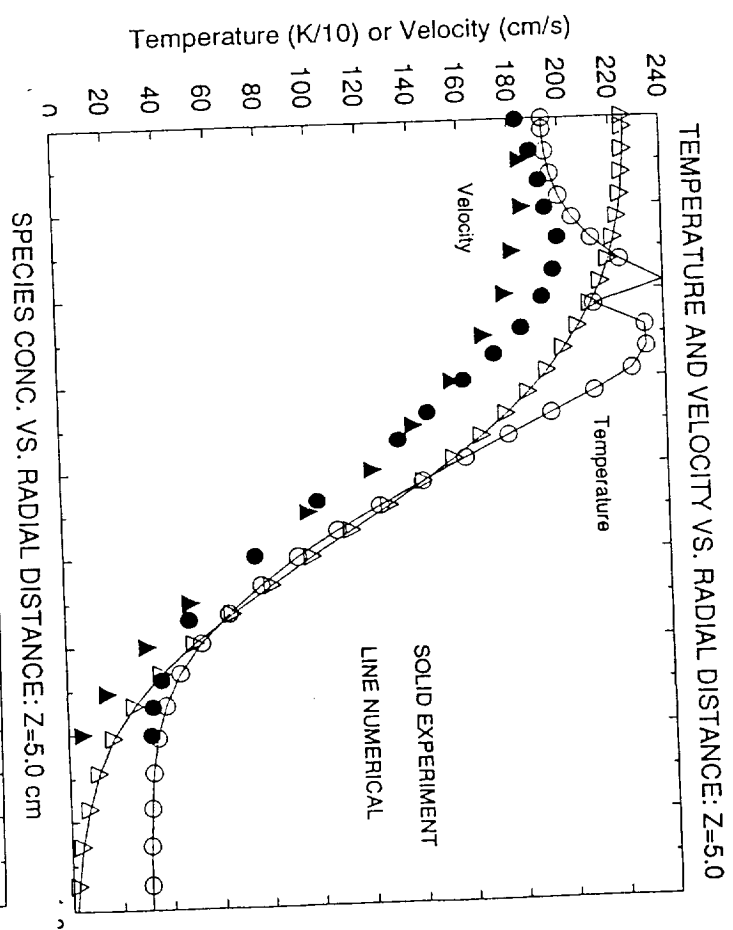
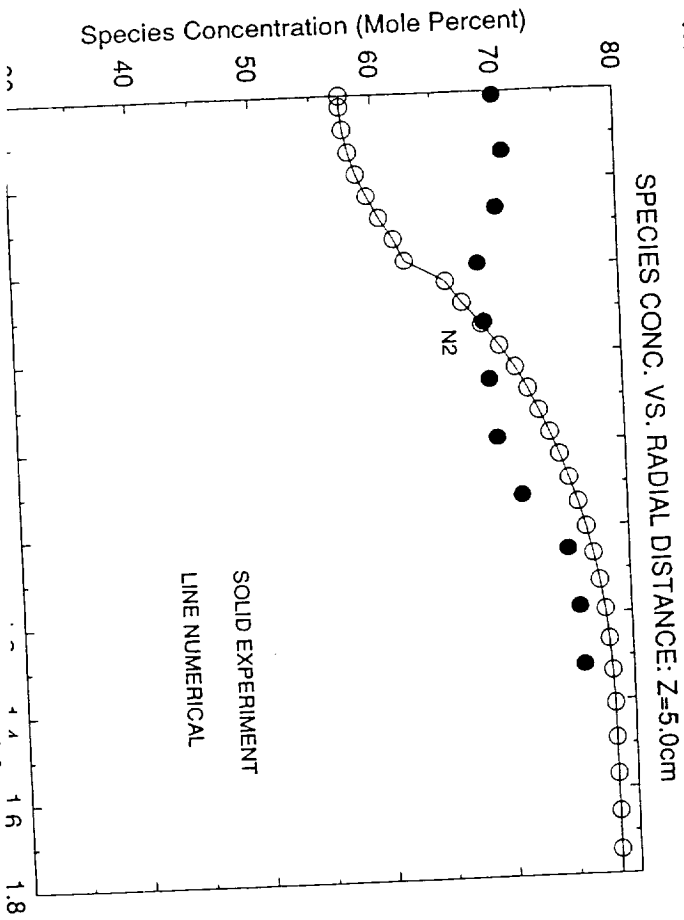


Fig. 6



17

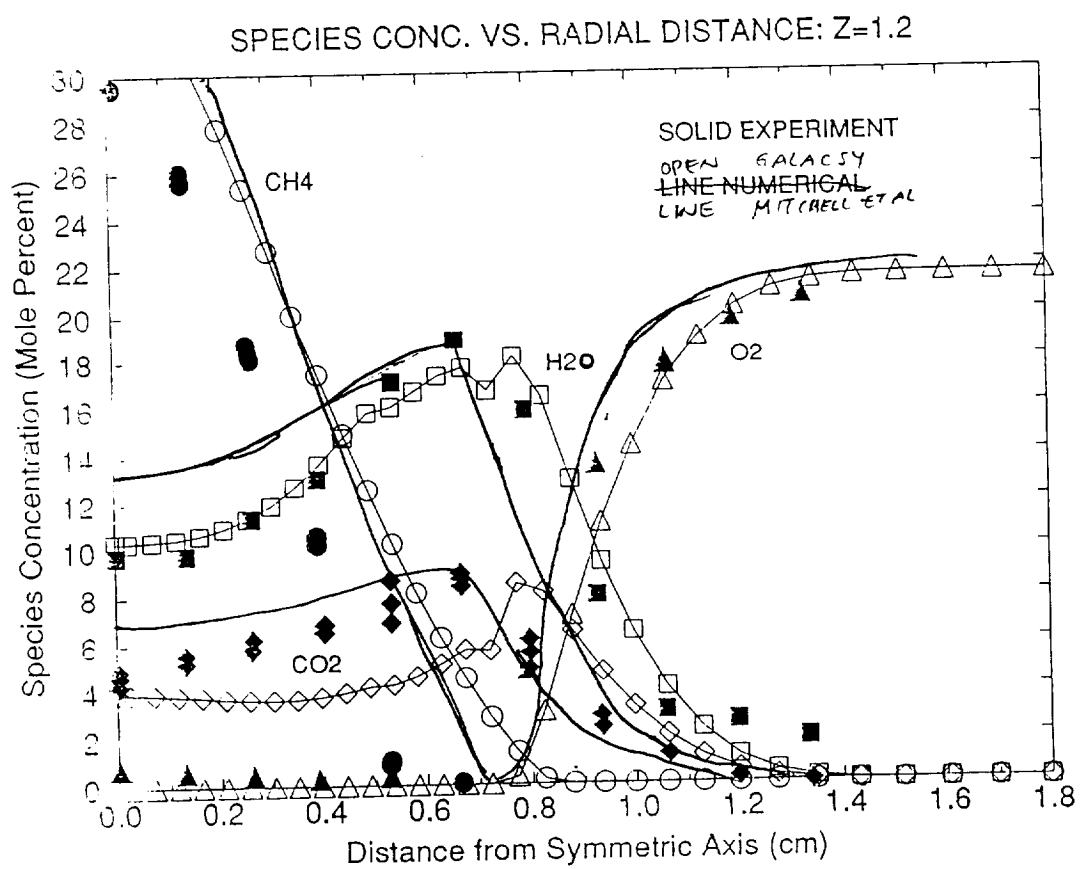
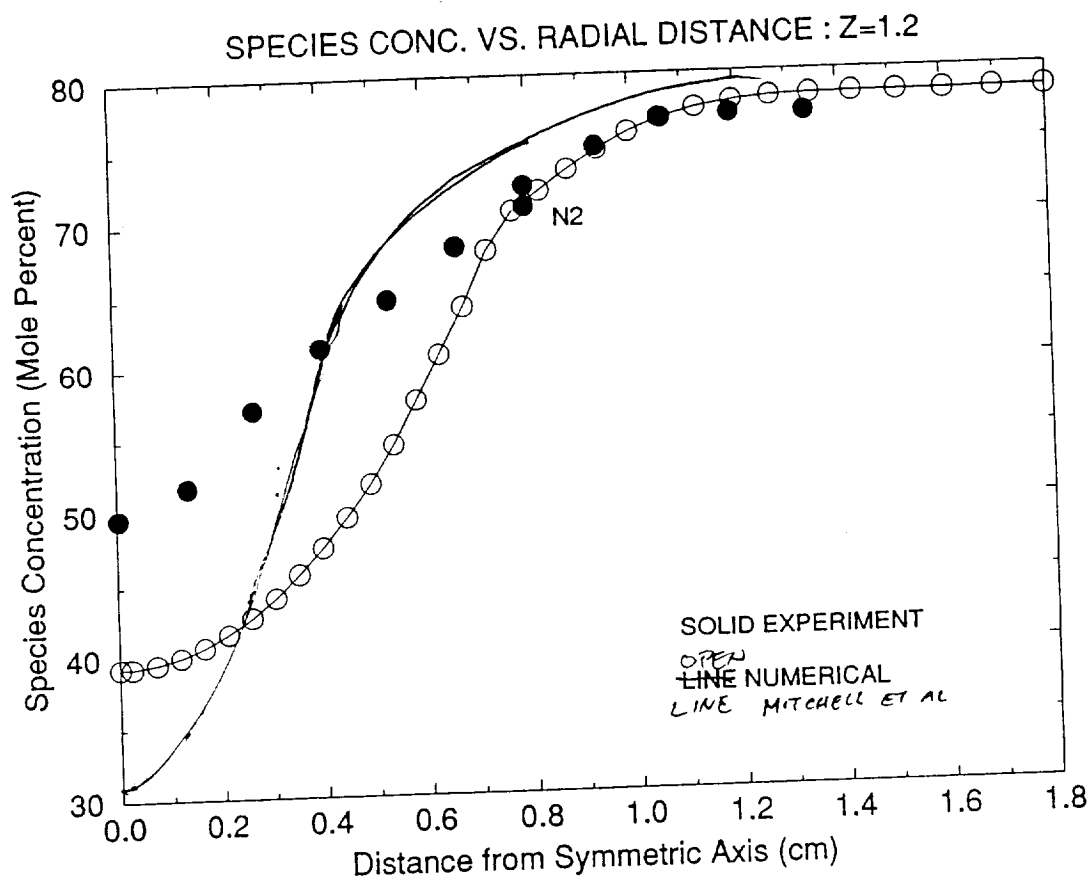


Fig. 8

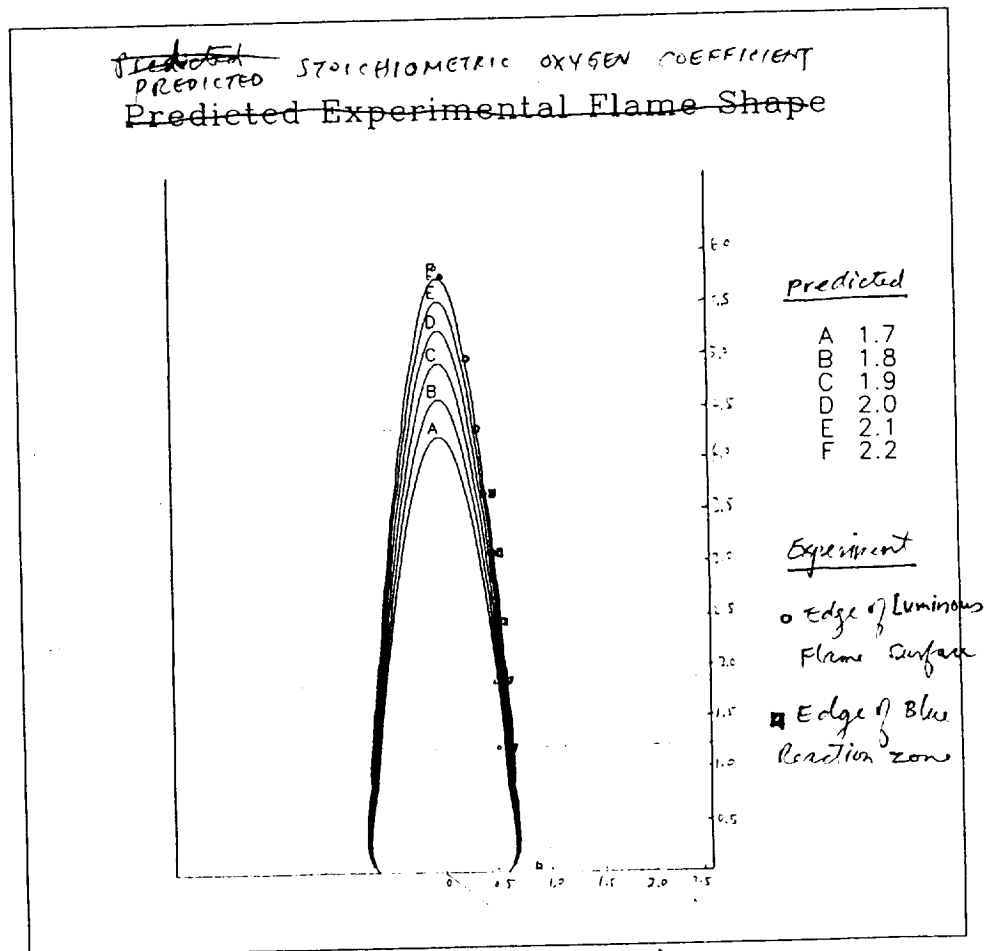


Fig. 9